A Finite-difference formulation of elastic rod for the design of actively bent structures

B. D'Amico[a,*], H. Zhang[a], A. Kermani[a]

[a] *School of Engineering and the Built Environment, Edinburgh Napier University, Edinburgh, UK*

Abstract

A discrete formulation of elastic rod has been tailored for the particular design task of geometric modelling, form finding and analysis of actively bent structural systems. The rod element is fully described by using vector based quantities, hence making it easy to implement and be suitable for explicit resolution methods such as the Dynamic Relaxation (DR). From this point of view, the model under consideration aims to provide a natural enhancement, of existing DR schemes of elastic rods, primarily formulated for analysis/design of stressed spline structures with isotropic cross-section, whilst, the proposed formulation allows for the general case of initially straight rods with anisotropic cross-section and torsional stiffness effects, to be taken into consideration. In order to avoid numerical conditioning problems, the method adopts a reduced Degrees of Freedom approach, however, the design limitations usually involved with such an approach, are 'removed' by adopting the Bishop theory of framed curves, hence making it possible to reduce to only three (translations) the Degrees of Freedom to be explicitly computed by numerical integration of the corresponding acceleration terms.

Keywords: Active bending, Form finding, Discrete elastic rod, Dynamic Relaxation, Finite-difference-method

1. Introduction

In the context of Architectural Geometry [1], the development of numerical tools, to assist the design and form exploration of actively bent structures, is gaining

*Corresponding author, telephone: +44 (0) 131 455 2249

Email addresses: bernardinodamico@gmail.com, b.d'amico@napier.ac.uk (B. D'Amico), j.zhang@napier.ac.uk (H. Zhang), a.kermani@napier.ac.uk (A. Kermani)

increasing interest [2, 3, 4, 5, 6]. According to Lienhard et al [7] the term 'Active-Bending' refers to those design cases in which the structural shape is obtained as a result of bending frameworks/assemblies of elastic members such as (but not limited to) rods or beams. Examples of constructing shelters and huts 'by bending' of branches, sticks or laths, probably date back to prehistoric times. Excepting those episodes of vernacular architecture, as for instance, the iconic mongolian Yurt [8]: aware-driven-designs examples of using bending as a self-forming process for the shape definition of roof structures (for both temporary [9, 10] or permanent use [11, 12, 13]) are fairly recent. Particularly, in the last few years, an increasing number of experimental pavilions [14, 15, 16, 17, 18] have been built around the world, by academics/professionals, in (both) Architecture/Structural Engineering, mostly as a means of drawing attention on such a 'new' method of building 'through' bending.

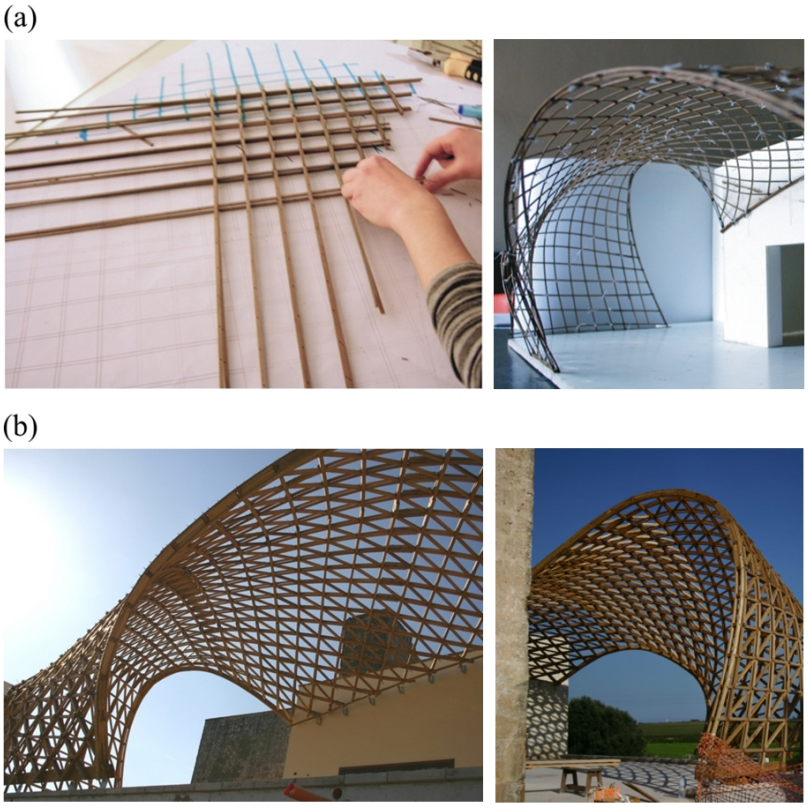

Figure 1: Trio grid-shell, Lecce, Italy, 2010, by: CMMKM Architettura e Design: (a) Physical (scale) models were extensively used during the design phase; (b) Realised structure.

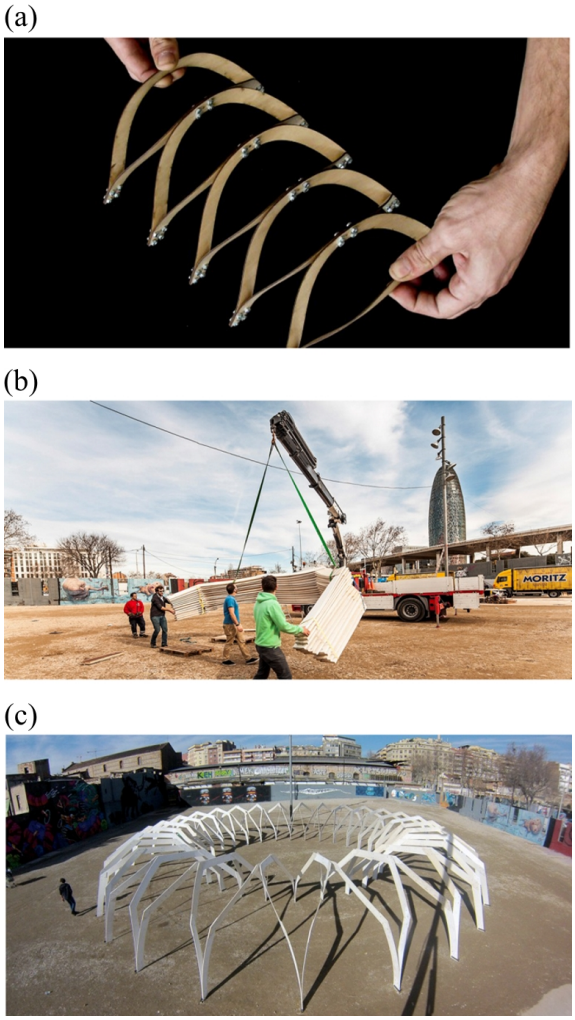

Figure 2: Pliable timber torus pavilion, Barcelona, 2014 [17], by: CODA (Computational Design Affairs): (a) Model prototype; (b) Construction phase; (c) Realised structure. Photos courtesy: David S. Anderson (WIT Press).

For the design of such actively bent systems, shape and material aspects are tightly connected through the particular construction (bending) process, meaning that: physical and/or numerical models are required to be used during the design process (see Figures 1, 2) in order to take the structural mechanical behaviour of the system into account while defining the architectural shape [19].

The discrete mathematical modelling of elastic rods is an expanding research field, finding application in several areas, for instance, in medicine [20], biology [21],

computer graphics [22, 23, 24], applied physics [25], computer aided design [26, 27] and structural engineering [28, 29]. Due to the large amount of literature on the topic: rather than providing a long list of previous works, it has been aimed (in the next subsections) to concentrate on the most relevant requirements upon which a model of discrete elastic rod suitable to aid the design of actively bent systems can be built. This will make possible to reduce the number of existing contributions to only few, as those most relevant to our need. In particular: a set of 'main' references throughout the paper is represented by the works of Adriaenssens and Barnes on stressed spline structures [30, 31, 32].

1.1. Resolution method: Implicit or Explicit?

For the physical simulation of elastic rods, and (in general) for every procedure aimed to numerically solve systems of ordinary and partial differential equations, implicit methods are preferred over explicit ones in describing the system's transient behaviour over the time domain (pseudo-time for static analyses). Implicit methods are generally preferred as they allow for larger (numerically stable) time increments to be considered and are insensitive to *numerical stiffness*. Emblematic in this regard is, for instance, the introduction to the Computer Graphic community of implicit integration methods for physically-based cloth simulation [33]. On the other hand, explicit methods have their own advantages, in particular: for those cases in which the given initial condition is 'very far' from the equilibrium solution, explicit formulations are more advantageous, since, the root-finding algorithm (e.g. the well known Newton-Raphson) allowing to 'implicitly' proceed over each time increment, works very well (quadratic convergence) when the integrating function is convex, whilst it is likely to fail otherwise.[1] This is a common situation when dealing with form finding analyses, in which, the problem's unknowns (namely, the structural shape) is sought by initializing the analysis with an arbitrary geometry, likely to experience gross deformations in converging to the equilibrium shape. This may explain the reason why, an explicit integration method such as the Dynamic

[1] In some cases such a 'limitation' inherent to implicit methods can have useful applications, as for instance, in the field of structural analysis, the critical buckling load of a structure can be obtained as the load increment at which the analysis fails to converge, since at that point the load-displacement curve becomes flat. Such a method was adopted, for instance, for the structural analysis of the Mannheim Multihalle grid-shell [11].

Relaxation (DR) is a standard procedure in the form finding/analysis of tension structures [34].

Clarified that the choice of an explicit or implicit resolution method will mainly depend upon the problem to be solved, for what we are concerned in here regarding actively bent (and twisted) structural systems, the following considerations can be made:

- For a 'pure' simulation of the structure's physical behaviour, e.g. in order to simulate the construction (bending) process [35] or for instance, to assess the structure's behaviour under working loads, an implicit method will be more advantageous. In such a case, stiffness parameters will be physically meaningful, as well as the mass parameter (in case of dynamic analyses).

- On the other hand, for 'design-oriented' problems, e.g. form finding analyses, the geometrical shape (rather than stresses and deformations) is the main unknown in the problem. Accordingly, an explicit method will certainly be more tenacious in seeking a solution, and in such a case: masses, time-step size and stiffness parameters can have no physical meaning at all but will be (likely) set according to prescribed design parameters and/or numerical stability issues.

1.2. Discrete formulation: 3, 4 or 6 Degrees of Freedom?

According to continuum mechanics theory, a rod or beam is a three-dimensional object having one dimension (length) L much bigger than the other two. For instance, in case of rectangular cross-section, with b and h the cross-sectional width and height respectively:

$$L \gg b \quad ; \quad L \gg h \tag{1}$$

From Kirchhoff [36] and Cosserat [37] theories of elastic rods (see Antman: [38]) such a three-dimensional object can be mathematically modelled as a one-dimensional entity, by considering a parametric curve in the Euclidean space, corresponding to the rod's centreline, with $\bar{r}$ the position vector of the material point along the curve. Assuming, for instance, the arclength $s \in [0, L]$ as a parameter:

$$\bar{r}(s) = \{r_x(s), r_y(s), r_z(s)\} \tag{2}$$

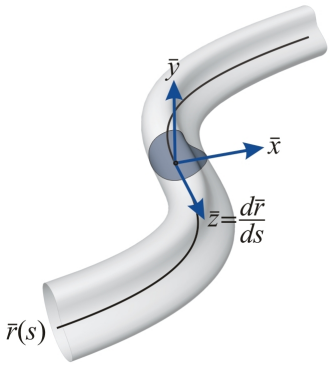

Figure 3: Continuous model of elastic rod by means of: a parametric curve $\bar{r}(s)$, representing the rod's centreline, and a moving frame $\{\bar{x}, \bar{y}, \bar{z}\}$ representing the material cross-section.

In addition, an orthonormal frame is introduced to represent the orientation of the rod's cross-section along the curve.

The choice of the local frame is not unique, and more details in regard will be given in section *3.3*. For now we consider a *material* frame $\{\bar{x}, \bar{y}, \bar{z}\}$ consisting of a unit vector $\bar{z}(s)$ tangent to the rod's centreline:

$$\bar{z}(s) = \frac{\partial \bar{r}}{\partial s} \tag{3}$$

thus coinciding with the tangent unit vector of the Frenet-Serret frame [39], and two *directors*, $\bar{x}(s)$ and $\bar{y}(s)$, defining the *Principal Axes* associated with the second moments of area I_x and I_y of the cross-section (see Figure 3). Noting that, as in the classic (EulerBernoulli/Saint-Venant) theory of beam, the plane of the cross-section is assumed to remain orthogonal to the rod's centreline.

Such a basic description of the rod's continuum, is the starting point from which an approximate (numerically solvable) discrete model can be built up. Assuming the rod's centreline $\bar{r}(s)$ represented by a discrete set $\mathbf{r}$ of $n+1$ nodes:

$$\mathbf{r} = \{\bar{r}_0 \dots \bar{r}_i \dots \bar{r}_n\} \tag{4}$$

If stiffness values are provided, relations can be built between the rod's geometry (node's position and cross-section orientation) and the corresponding nodal forces (reactions) by applying concepts of stain energy minimization. For instance, assuming a piecewise cubic spline interpolation of the node set $\mathbf{r}$, the ith piece of

rod's centreline is given by:

$$\bar{r}_i(t) = (2t^3 - 3t^2 + 1)\bar{r}_i + (t^3 - 2t^2 + t)\bar{m}_i + (-2t^3 + 3t^2)\bar{r}_{i+1} + (t^3 - t^2)\bar{m}_{i+1} \quad (5)$$

with:

$$i = 0, \ldots, n-1 \quad ; \quad t \in [0, 1] \quad (6)$$

thus, the piece of curve is uniquely defined by: the end nodes $\bar{r}_i = \bar{r}_i(0)$ and $\bar{r}_{i+1} = \bar{r}_i(1)$ and by the end tangent vectors $\bar{m}_i$ and $\bar{m}_{i+1}$.

If we express the orientation of the element's end tangent vector $\bar{m}_i = \bar{z}_i|\bar{m}_i|$ in terms of *local rotational displacements* θ_x, θ_y [40] as shown in Figure 4a, the piece of spline from i to $i+1$ resembles the *shape function* of a Finite beam Element with 12 Degrees of Freedom (DoF) or more precisely, with 6 DoF per node: 3 translations, corresponding to the Cartesian components of the node, and 3 rotations, corresponding to the two angles (θ_x and θ_y) defining the local orientation of $\bar{z}$ around $\bar{p}_i$ (see Figure 4a) plus a twisting angle, defining the orientation of the local frame around its own $\bar{z}$ axis.

The idea of having at least 6 DoF per node, to 'completely' describe the mechanical behaviour of a beam element, is widely accepted in the Structural Engineering community.

In general, Computer Graphic models are focused on defining reduced DoF formulations, with the main scope of reducing computational time by avoiding rotational DoF at the expense of quantitative accuracy (see for instance [24]). In fact, as noted by Adriaenssens and Barnes [31]: *"...it is often the coupling of these* (rotational DoF) *with axial stiffness and translational DoF, which cause conditioning problems in numerical explicit methods such as Dynamic Relaxation"*. Practically, the coupling between translational and rotational DoF requires a smaller size of the time-steps in explicit resolution methods.

Common formulations of discrete elastic rods with a reduced number of DoF, assume the material frame at a element level instead of at a node level [27] (see Figure 4b) so that the orientation of the tangent-to-centreline vector $\bar{z}$ is function of the node's position only (absence of shape functions) therefore, the tangent's orientation does not need to be searched explicitly. Accordingly, the only remaining rotational DoF is the angles of twist of the material frame. As in [22], we keep the local frame at a node level, but enforce the tangent direction $\bar{z}$ by means of *local spline interpolation.*

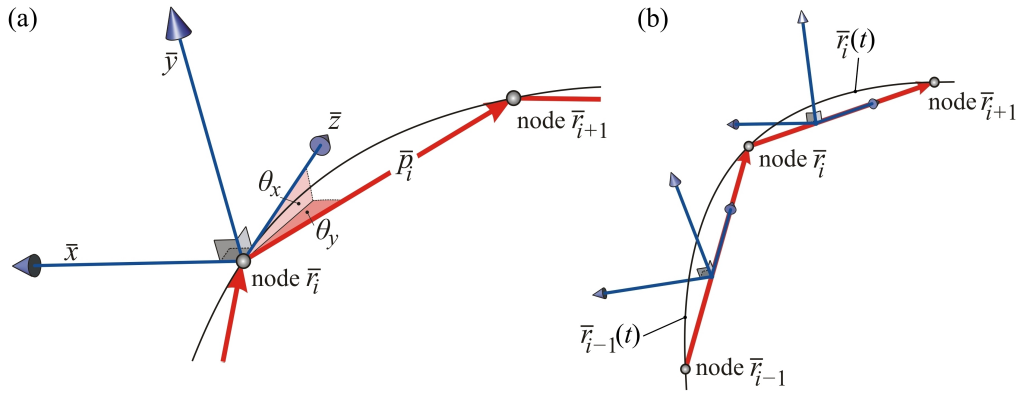

Figure 4: Discrete elastic rod: (a) *Total* DoF formulation; (b) *Reduced* DoF formulation.

Furthermore, if torsional stiffness is neglected and the rod model is restricted to the case of isotropic cross-section ($I_x = I_y$) the DoF can be reduced to only three (translations) [31]. This corresponds to the degenerate case, in which, every couple of orthogonal directors ($\bar{x}$, $\bar{y}$) around the unit tangent $\bar{z}$, is a valid couple of *Principal Axes* (e.g. in case of circular cross-section). Also, for naturally curved rods with isotropic cross-section, torsional stiffness can be taken into account by considering translational DoF only [32].

2. Problem statement

Established that: a 'design-oriented' formulation of discrete elastic rod (e.g. for form finding analyses) of actively bent structural systems, will:

- Adopt an explicit integration method
- Avoid rotational DoFs in explicit form.
- Be able to simulate torsional stiffness.
- Not be restricted to the particular case of naturally curved rods.
- Be able to simulate cross-section anisotropy ($I_x \neq I_y$).

we note that, the first three points have been successfully addressed by the work of Adriaenssens and Barnes [31] and Barnes et al [32]. Accordingly, our contribution in here is, in practice, an extension of such previous works, to allow to take into account the 'general' case of naturally straight rods with anisotropic cross-section.

3. Theory

3.1. Dynamic Relaxation method

According to 'classic' (Stiffness Matrix) Finite Element Analysis procedures [41], the continuum model, of the mechanical system under consideration, is 'converted' into an equivalent discrete system of non-linear equations as follow:

$$\mathbf{K}\boldsymbol{x} = \mathbf{f} \tag{7}$$

In which: $\boldsymbol{x}$ represents the vector of nodal displacements, whilst $\mathbf{K}$ is the *global* stiffness matrix and $\mathbf{f}$ the vector of applied nodal forces (and constraints' reactions). In general, a static solution to Eq. (7) is pursued by operations of matrix inversion of the kind: $\boldsymbol{x} = \mathbf{K}^{-1}\mathbf{f}$. On the other hand, in the Dynamic Relaxation method (DR) the original system of non-linear Eq. (7) is transformed into a system of equations of motion:

$$\mathbf{M}\boldsymbol{a} + \mathbf{C}\boldsymbol{v} + \mathbf{K}\boldsymbol{x} = \mathbf{f} \tag{8}$$

by introduction of a matrix $\mathbf{M}$ of lumped nodal masses and a matrix $\mathbf{C}$ of viscous damping forces, required to 'force' the system converging to a rest configuration.[2] Therefore, computing the displacements $\boldsymbol{x}$ by explicit numerical integration of the acceleration and velocity terms: $\boldsymbol{a}$ and $\boldsymbol{v}$ respectively. Let note that a matrix of lumped masses must be appropriately chosen to consent fast numerical convergence and at the same time avoiding numerical instability. In particular, small fictitious masses would allow for a reduced number of iterations, however under a certain critical value the analysis may fails to converge. For an arbitrary time interval Δt (required to perform the numerical time-integration) the smallest, numerically stable, mass component to consider for the ith node it is provided by Barnes (see [43]) as a value which is directly proportional to the greatest direct stiffness expected to occur (for the ith node) during the whole analysis.

Eq. (8) can be expressed, at time t, in the following form:

$$\mathbf{M}\boldsymbol{a}^t + \mathbf{C}\boldsymbol{v}^t = \mathbf{R}^t \tag{9}$$

[2] The Kinetic Damping method [42] can be used as alternative to (or in conjunction with) viscous damping.

thus, with $\mathbf{R} = \mathbf{f} - \mathbf{K}\boldsymbol{x}$ representing the vector list of out-of-balance forces (residuals) as resultant of the applied loads/constraints forces $\mathbf{f}$ plus member's internal reactions $\mathbf{K}\boldsymbol{x}$. By making the stiffness matrix disappearing (see Eq. (9), the system can be solved at a node-by-node level (this is a peculiar characteristic of the DR method) hence, the main task reduces to the computing, at each time increment, of the residual vector force $\bar{R}_i$ for the ith node:

$$\mathbf{R} = \left\{ \bar{R}_0 \dots \bar{R}_i \dots \bar{R}_n \right\} \tag{10}$$

This task is fully addressed in the following subsections and represents the core of the present research.

3.2. Enforcing tangents

As highlighted in section *1.2*, in order to implement a *reduced* DoF formulation of discrete elastic rod, the tangent-to-centreline orientation needs to be expressed as a function of the nodes' position only. This requirement is fulfilled by spline interpolation of the whole node set $\mathbf{r}$. Several interpolation methods are available, and probably, the most 'obvious' choice would be to use a formulation based on minimization of the bending and twisting energy, as for instance, a third-order *natural spline* [44]. However, one of the requirement for developing the rod's model under description is that of having the tangent vectors $\bar{m}_i$ lying parallel to the plane defined by the three consecutive nodes $\bar{r}_{i-1}$, $\bar{r}_i$ and $\bar{r}_{i+1}$ (the reason for such a requisite will become clear in a later part of the present section) and this is generally not the case for a *natural spline*, interpolating more than three nodes arbitrarily set in the Cartesian space. Consequently, the Catmull-Rom method [45] is adopted in here, according to which, for the pieces of cubic spline expressed in isoparametric form ($t \in [0, 1]$) the tangent vector at the ith node is:

$$\bar{m}_i = \frac{\bar{r}_{i+1} - \bar{r}_{i-1}}{2} \quad ; \quad \bar{z}_i = \frac{\bar{m}_i}{|\bar{m}_i|} \tag{11}$$

As can be clearly seen from the first of Eqs. (11): for boundary nodes $\bar{r}_0$ and $\bar{r}_n$, the Catmull-Rom algorithm requires the definition of two additional control points (nodes) in order to provide the tangent vectors $\bar{m}_0$ and $\bar{m}_n$. Nevertheless, it can be easily demonstrated that Eq. (11) corresponds to the tangent vector (in $\bar{r}_i$) of a *natural spline* passing through three consecutive nodes $\bar{r}_{i-1}$, $\bar{r}_i$ and $\bar{r}_{i+1}$. In fact,

by solving the tridiagonal system associated with the corresponding three-nodes *natural spline* (see [44]):

$$\begin{bmatrix} 2 & 1 & \\ 1 & 4 & 1 \\ & 1 & 2 \end{bmatrix} \cdot \begin{Bmatrix} \bar{m}_{i-1} \\ \bar{m}_i \\ \bar{m}_{i+1} \end{Bmatrix} = 3 \begin{Bmatrix} \bar{r}_i - \bar{r}_{i-1} \\ \bar{r}_{i+1} - \bar{r}_{i-1} \\ \bar{r}_{i+1} - \bar{r}_i \end{Bmatrix} \tag{12}$$

we obtain:

$$\begin{aligned} \bar{m}_{i-1} &= -\frac{5}{4}\bar{r}_{i-1} + \frac{3}{2}\bar{r}_i - \frac{1}{4}\bar{r}_{i+1} \\ \bar{m}_i &= -\frac{1}{2}\bar{r}_{i-1} + \frac{1}{2}\bar{r}_{i+1} \\ \bar{m}_{i+1} &= \frac{1}{4}\bar{r}_{i-1} - \frac{3}{2}\bar{r}_i + \frac{5}{4}\bar{r}_{i+1} \end{aligned} \tag{13}$$

Accordingly: the first of Eqs. (13) is used for computing the tangent vector $\bar{m}_0$ at the rod's start node $\bar{r}_0$, whilst the third of Eqs. (13) provides the tangent vector $\bar{m}_n$ at the rod's end node $\bar{r}_n$. Needless to say that Eq. (11) and the second of Eqs. (13) are the same expression.

It is important to note that: the rod's start/end tangents, provided by local *natural spline* interpolation (first, and third of Eqs. (13)) are based upon assumption of null second derivatives at the start/end nodes of the first/last pieces of spline $\bar{r}_0(t)$ and $\bar{r}_{n-1}(t)$ respectively:

$$\frac{\partial^2 \bar{r}_0}{\partial(t=0)} = \frac{\partial^2 \bar{r}_{n-1}}{\partial(t=1)} = \bar{0} \tag{14}$$

and: since the second derivative of the rod's centreline (Eq. (2)) corresponds to the magnitude of the rate of change of the unit tangent vector $\bar{z}$, or in simpler words, to the curvature κ [38] :

$$\left| \frac{\partial^2 \bar{r}}{\partial s^2} \right| = \kappa = \frac{M}{EI} \tag{15}$$

the described method for tangents' enforcement implies to assume zero curvatures at the start/end of the rod. Hence, for bending stiffness values $EI \neq \infty$, it implies to assume null bending moments (M) at the rod's ends. From a mechanical point of view, this is only true for particular boundary conditions, e.g. in case of pinning restraints. However, if rotational constraints are required to be considered at the boundary of the rod's centreline, this can be done by imposing translational constraints at 'pairs' of consecutive nodes (as proposed in [31]). An example, in

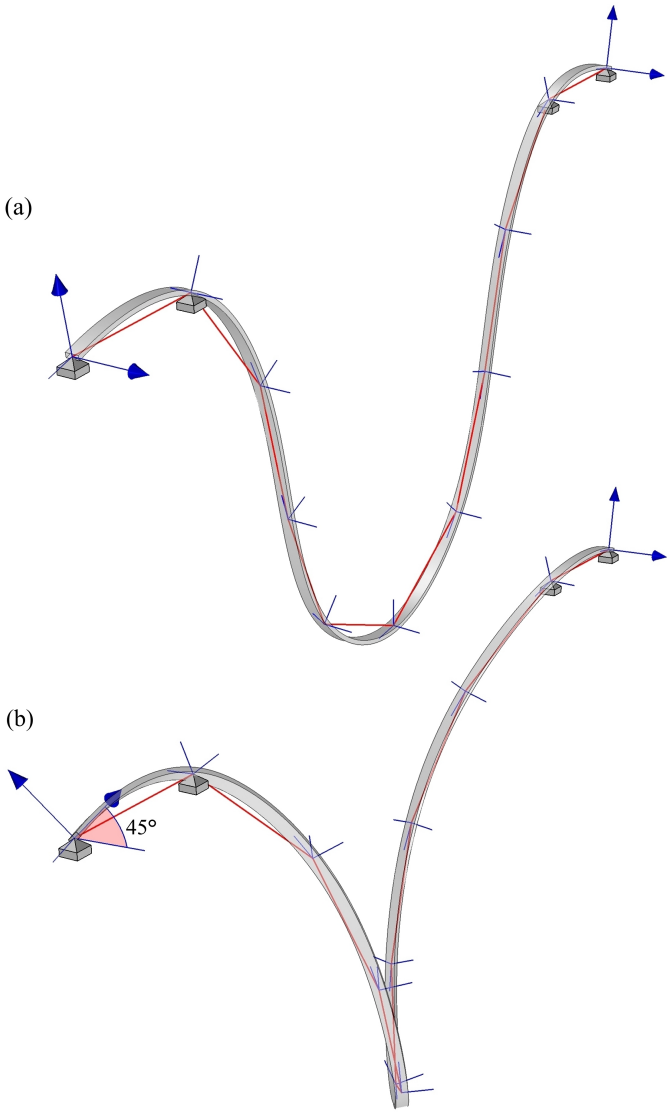

Figure 5: Discrete elastic rod: (a) An initially straight rod is bent into shape by assuming clamping end conditions; (b) Torque is introduced to the previously bent rod by imposing a 45° twist to its end.

this regard, is shown in Figure 5a where, 'clamps' are simulated at the ends of an initially straight rod by restraining the translational DoF of the first two (and last two) nodes, thus, in a manner 'consistent' with the assumption of zero curvatures at the boundary nodes (see Eq. (14)).

3.3. Quasi-static treatment of twisting DoF

By enforcing the tangent-to-centreline vectors $\bar{z}$ as a function of the nodes' position, the only remaining rotational DoF is the angle of twist of the material frame around its own $\bar{z}$ axis. Following the work of Bergou et al [23], the unit vectors $\bar{x}(s)$ and $\bar{y}(s)$, representing the material cross-section orientation around the centreline curve $\bar{r}(s)$, can be computed by aid of the *Bishop* theory of framed curves [46].

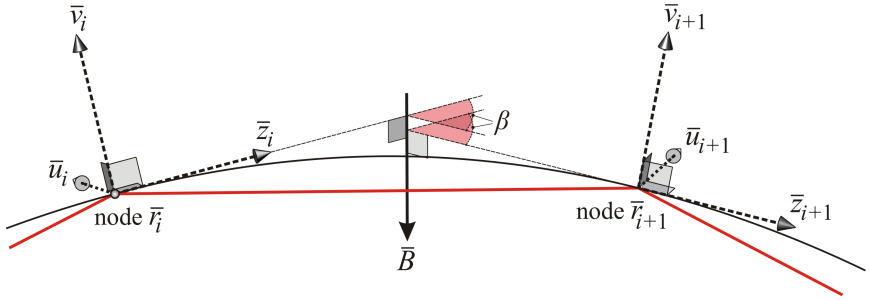

Figure 6: Parallel transported (Bishop) frame along the rod's centreline by means of: a rotation axis (represented by the unit vector $\bar{B}$) and a rotation angle β.

Accordingly, the whole curve domain $[0, L]$ can be 'framed' by 'prescribing' the material frame directors $\{\bar{x}(0), \bar{y}(0)\}$ at the rod's starting node $\bar{r}(0)$, and assuming a scalar value φ_L representing the angle of twist of the material frame around the centreline curve at the rod's end node $\bar{r}(L)$. In practice, the 'framing' procedure for our discrete rod, consists in applying the following two consecutive steps:

- Firstly, an orthonormal Bishop frame $\{\bar{u}_0, \bar{v}_0, \bar{z}_0\}$ is set at the rod's start node $\bar{r}_0$ according to the material frame directions $\{\bar{x}_0, \bar{y}_0, \bar{z}_0\}$. Then, as described in [47], such a Bishop frame is *parallely transported* on the successive node $\bar{r}_1$ (and so on, up to $\bar{r}_n$) by rotating it around a unit vector $\bar{B}$ by an angle β. With the help of Figure 6, and referring to the general case of a Bishop frame transported from node $\bar{r}_i$ to the successive node $\bar{r}_{i+1}$: the unit vector $\bar{B}$ and rotation angle (β) are both functions of the tangent vectors $\bar{z}_i$ and $\bar{z}_{i+1}$:

$$\bar{B} = \frac{\bar{z}_i \times \bar{z}_{i+1}}{|\bar{z}_i \times \bar{z}_{i+1}|} \quad ; \quad \beta = arcos(\bar{z}_i \cdot \bar{z}_{i+1}) \tag{16}$$

  With $\bar{B}$ and β so found, the described rotation can be performed by assembling of a rotation matrix, or by means of quaternions: (β, B_x, B_y, B_z).

Moreover, in the degenerate case of a straight rod ($\bar{z}_{i+1} \approx \bar{z}_i \Rightarrow \beta \approx 0$) the vector product in the first of Eqs. (16) is obviously undefined. If that is the case, then the following exception applies:

$$\{\bar{u}_{i+1}, \bar{v}_{i+1}, \bar{z}_{i+1}\} = \{\bar{u}_i, \bar{v}_i, \bar{z}_i\} \tag{17}$$

- Once the discrete rod is framed along the whole node set, the second step consists of rotating each Bishop frame around its tangent axis $\bar{z}$ in order to obtain the corresponding material frame. The following rotation angle φ_i will be considered to obtain the material frame at the ith node (see Figure 7):

$$\varphi_i = \varphi_L \frac{\sum_{j=1}^{i} |\bar{r}_j - \bar{r}_{j-1}|}{\sum_{i=1}^{n} |\bar{r}_i - \bar{r}_{i-1}|} \tag{18}$$

For instance, the material frame $\{\bar{x}_n, \bar{y}_n, \bar{z}_n\}$ at the rod's end node ($\bar{r}_n$) will be obtained by rotating the (previously found) Bishop frame of φ_L radiant. On the opposite, the material frame at the rod's start node $\bar{r}_0$ will be coincident with the Bishop frame. Essentially: φ_L is a scalar, by which, torsional constraints can be imposed at the ends of rod. See for instance Figure 5b in which, a twist $\varphi_L = 45°$ is imposed at the (previously bent) rod with clamped ends.

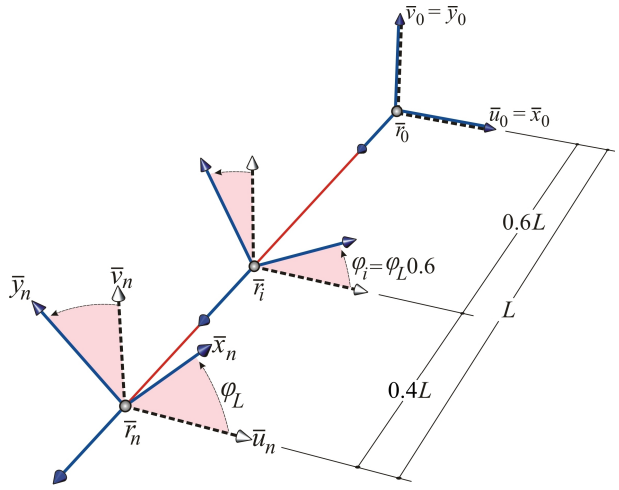

Figure 7: Quasi-static treatment of twisting DoF: the material frame at the ith node is obtained by rotating (of φ_i radiant) the Bishop frame around its tangent unit vector $\bar{z}_i$.

The described procedures for enforcement of the unit tangents and material frames (subsections *3.2* and *3.3*) are performed at each time increment of the DR analysis, according to the updated nodal positions, which are the only unknowns that need to be sought by explicit numerical integration of the acceleration terms. In other words: the numerical scheme under proposal allows to reduce, in practice, the number of DoF-per-node to only 3 (translations). A last remark to implement the described quasi-static treatment of the material frame, relates to the time-update of the control frame $\{\bar{x}_0 \equiv \bar{u}_0, \bar{y}_0 \equiv \bar{v}_0, \bar{z}_0\}$. This task is performed by applying the parallel transport procedure to the control frame at each time increment, e.g. from time "t" to time "$t + \Delta t$":

$$\bar{B}^* = \frac{\bar{z}_0^t \times \bar{z}_0^{t+\Delta t}}{|\bar{z}_0^t \times \bar{z}_0^{t+\Delta t}|} \quad ; \quad \beta^* = arcos(\bar{z}_0^t \cdot \bar{z}_0^{t+\Delta t}) \tag{19}$$

and then, with the control frame so updated, the parallel transport is applied over space (as already described) to the entire rod.

3.4. Computing residuals

In order to trace the system behaviour, hence, eventually obtaining the geometry of rest configuration, the out-of-balance forces $\bar{R}_i$ need to be computed for each node, at each time increment. Such residual at the ith node, is obtained by vector summation of the axial reactions of the links surrounding the node, plus a shear vector force due to the presence of bending and torsional stiffnesses EI_x, EI_y and GJ respectively. The axial reactions are computed as a function of the shortening/elongation and (real or fictitious) axial stiffness EA of the links surrounding the ith node, hence by taking into account pairs of consecutive nodes, e.g. ($\bar{r}_i$, $\bar{r}_{i+1}$). By contrast, the out-of-balance shear forces are obtained by considering local sets of three consecutive nodes ($\bar{r}_{i-1}$, $\bar{r}_i$, $\bar{r}_{i+1}$) along the rod. With the help of Figure 8, and following [31], the shear reactions $\bar{S}_a$ and $\bar{S}_b$ are obtained as (lever-arm) function of the moment $\bar{M}$ which in turn, is obtained in here as a function of combined bending plus torsion.

Indicating with $\bar{p}_a$ and $\bar{p}_b$ the vector-links surrounding the ith node, the free body shears $\bar{S}_a$ and $\bar{S}_b$ shown in Figure 8b are:

$$\bar{S}_a = \bar{u}_a \frac{|\bar{M}|^2 |\bar{p}_a \times \bar{u}_a|}{|\bar{p}_a| \left[\bar{M} \cdot (\bar{p}_a \times \bar{u}_a)\right]} \quad ; \quad \bar{u}_a = \frac{\bar{M} \times \bar{p}_a}{|\bar{M} \times \bar{p}_a|} \tag{20}$$

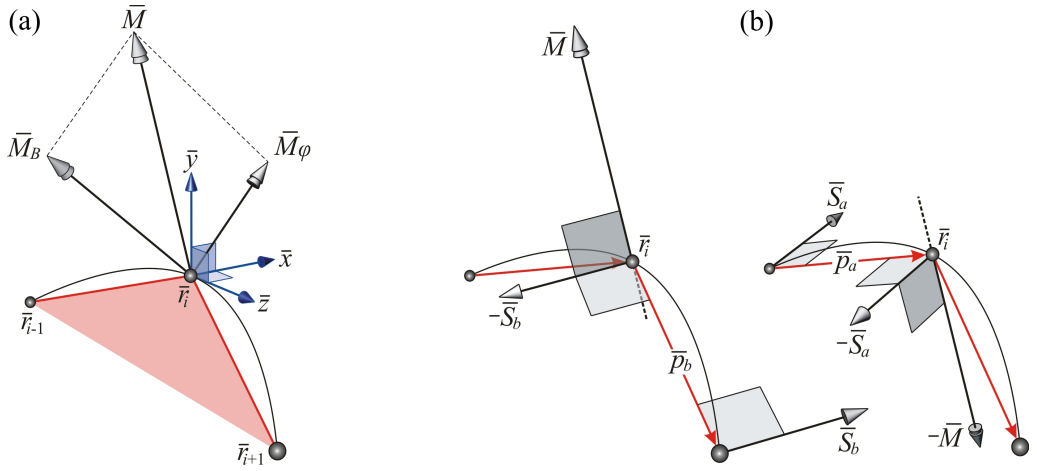

Figure 8: Out-of-balance shears: (a) $\bar{M} = \bar{M}_B + \bar{M}_\varphi$; (b) Shears $\bar{S}_a, \bar{S}_b$ as a function of $\bar{M}$.

Eqs. (20), whose derivation can be found in [40], equally applies to $\bar{S}_b$ by replacing $\bar{p}_a$ with $\bar{p}_b$ (and $\bar{u}_a$ with $\bar{u}_b$). As shown in Figure 8a: the moment $\bar{M}$ is obtained by vector summation of the moment due to combined bending ($\bar{M}_B$):

$$\bar{M}_B = EI_x\bar{\kappa}_x + EI_y\bar{\kappa}_y \tag{21}$$

plus the vector ($\bar{M}_\varphi$) due to torsion, which is obtained by considering the angle of twist per unit length of the two elements surrounding the ith node:

$$\bar{M}_\varphi = GJ\left[arcos(\bar{y}_{i-1}\cdot\bar{y}_i)\frac{\bar{p}_a}{|\bar{p}_a|^2} - arcos(\bar{y}_i\cdot\bar{y}_{i+1})\frac{\bar{p}_b}{|\bar{p}_b|^2}\right] \tag{22}$$

Noting that: $\bar{M}_\varphi$ is always lying parallel to the plane defined by the three nodes $(\bar{r}_{i-1}, \bar{r}_i, \bar{r}_{i+1})$ and in the case of $\bar{p}_a$ parallel to $\bar{p}_b \Rightarrow \bar{M}_\varphi = \bar{0}$. Also, the vector of combined bending moment ($\bar{M}_B$) is assumed aligned on the local plane $(\bar{x}, \bar{y})$ of the rod's cross-section. Accordingly, the curvature vectors in Eq. (21) are:

$$\bar{\kappa}_x = (\bar{\kappa}\cdot\bar{x})\bar{x} \quad ; \quad \bar{\kappa}_y = (\bar{\kappa}\cdot\bar{y})\bar{y} \tag{23}$$

with the vector $\bar{\kappa}$ oriented parallel to the $(\bar{x}, \bar{y})$ plane of the material frame (as for $\bar{M}_B$). Such a curvature vector $\bar{\kappa}$, can be obtained by scaling, of κ amount, the unit vector normal to the local plane defined by the three nodes $\bar{r}_{i-1}, \bar{r}_i$ and $\bar{r}_{i+1}$:

$$\bar{\kappa} = \kappa\frac{\bar{p}_a \times \bar{p}_b}{|\bar{p}_a \times \bar{p}_b|} \tag{24}$$

and the scalar κ obtained by assuming a circular arch passing through the same three nodes (see Figure 9). According to [31]:

$$\kappa = \frac{2sin(\alpha)}{|\bar{r}_{i+1} - \bar{r}_{i-1}|} \quad ; \quad \alpha = arcos\left(\frac{|\bar{p}_a|^2 + |\bar{p}_b|^2 - |\bar{r}_{i+1} - \bar{r}_{i-1}|^2}{2|\bar{p}_a||\bar{p}_b|}\right) \tag{25}$$

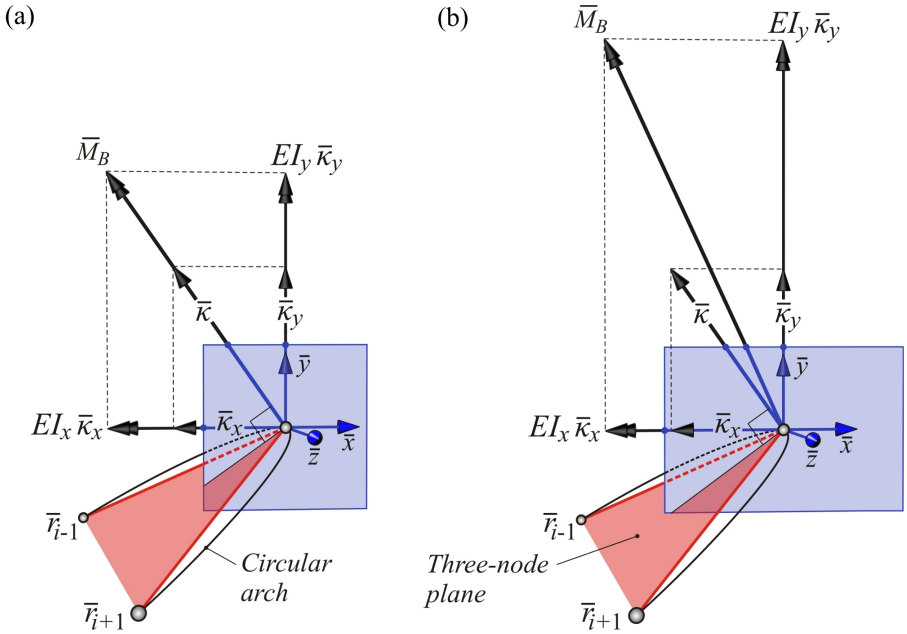

Figure 9: Cross-section: (a) Isotropic: $I_x = I_y$; (b) Anisotropic: $I_x \neq I_y$.

The assumption of $\bar{\kappa}$ as a vector orthogonal to the three-node plane (see Figure 9) is only valid if $\bar{z}$ results parallel to the three-node plane. This is always true, regardless of the material frame orientation, thanks to the Catmull-Rom algorithm for tangents enforcement (see Eqs. (11)). Let also highlight that: the curvature value provided by Eqs. (25) does not correspond to the second derivative of the Catmull-Rom spline (Eq. (15)). Nonetheless, the spline interpolation was adopted in here for the only task of enforcing the tangents' direction.

As it can be seen from Figure 9a: for isotropic cross-sections, the curvature vector $\bar{\kappa}$ and the vector of bending moment $\bar{M}_B$ are both aligned along the same direction. Furthermore, if no torque is taken into account ($|\bar{M}_\varphi| = 0 \Rightarrow \bar{M} = \bar{M}_B$), in addition to cross-section isotropy ($I_x = I_y$) then, the free body shears ($\bar{S}_a, \bar{S}_b$) will be both aligned with the three-node local plane highlighted in Figure 9. In such a 'particular' case, the present elastic rod formulation corresponds to the one

proposed by Adriaenssens and Barnes [31]. On the opposite, in case of cross-section anisotropy ($I_x \neq I_y$): $\bar{M}_B$ and $\bar{\kappa}$ will, in general, not be aligned (see Figure 9b) unless one of the cross-sectional *Principal Axes* ($\bar{x}$ or $\bar{y}$) occurs to be oriented normally (or parallel) to the three-node local plane.

A concluding remark, concerns the shear vector residuals provided by Eq. (20) to allow computer implementation of the described method. In fact, such equation only provides partial values of shear and they need to be properly added/subtracted to the shears computed from the surrounding nodes (plus, the links' axial reactions indeed). For instance, assuming to compute the total nodal shears ($\bar{S}_i$) in a 'procedural' way, starting from node $\bar{r}_0$ up to node $\bar{r}_n$, the following routine can be adopted (as proposed in [30]):

$$\begin{aligned} \bar{S}_{i-1} &= \bar{S}_{i-1} + \bar{S}_a \\ \bar{S}_i &= \bar{S}_i - \bar{S}_a - \bar{S}_b \\ \bar{S}_{i+1} &= \bar{S}_{i+1} + \bar{S}_b \end{aligned} \tag{26}$$

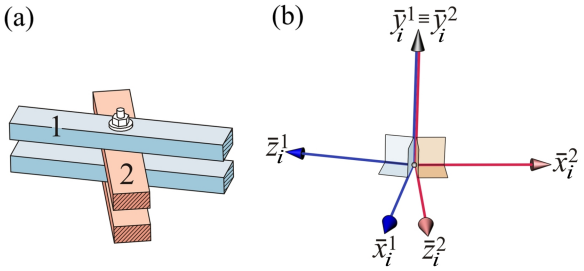

Figure 10: Cylindrical-hinge connection: (a) Real connection system; (b) Equivalent numerical model.

3.5. Constraints

Thanks to the adopted vector-based formulation, typical of DR schemes, prescribing local or global constraints results a pretty straightforward operation to perform. For instance, the coupling of translational DoF, between two or more rods joined together at the ith node, is simulated by assuming the total residual $\bar{R}_i$ obtained as vector summation of the $\bar{R}_i^j$ residual of the jth rod converging to the node:

$$\bar{R}_i = \sum_{j=1}^{n^\circ} \bar{R}_i^j \tag{27}$$

with n° indicating the total number of rods converging to the ith node. Further, if torsional constraints need to be taken into account, as for instance, to simulate the cylindrical-hinge mechanism occurring at the connections of post-formed grid-shells (see Figure 1), the material frame orientation, around the $\bar{z}_i$ tangent-to-centreline direction, is uniquely defined as the normal direction to both $\bar{z}_i^1$ and $\bar{z}_i^2$ as shown in Figure 10:

$$\bar{y}_i = \bar{z}_i^1 \times \bar{z}_i^2 \tag{28}$$

Interesting to note that: in the particular case of post-formed grid-shells, (see e.g. Figure 1) torsional constraints of the kind in Eq. (28) are applied to the entire node set. Accordingly, there will be no local frames left, whose orientation, need to be interpolated by parallel transport, hence making superfluous the whole procedure described in subsection *3.3*.

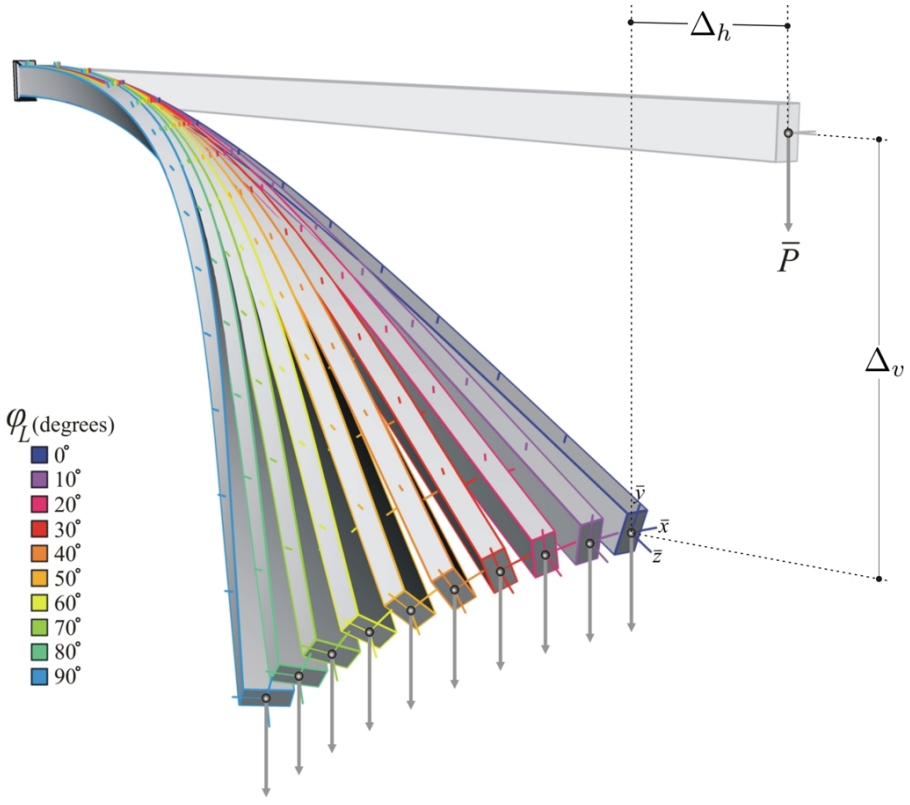

Figure 11: Lateral buckling of a cantilever beam with anisotropic cross-section ($I_x = 4I_y$).

4. Calculation

4.1. Cantilever beam

A simple test is provided in here to assess the accuracy of the 3 Dof formulation in comparison to a co-rotational beam-element with 6 DoF (described in [48]): A 10 m long cantilever beam is subjected to a vertical load $\bar{P} = 1$ kN at its free end. Axial stiffness $EA = 100$ MN, bending stiffnesses EI_x and EI_y of 100 kNm^2 and 25 kNm^2 were set respectively, as well as a torsional stiffness $GJ = 50$ kNm^2. The two cantilever's models (with three and six DoF) were both discretised into an increasing number (from 12 to 48) of evenly spaced elements, whose length is ranging form 833.333 mm (for the 12 elements model) down to 208.333 mm (for the 48 elements model). Both analyses were explicitly solved by adopting the fourth-order Runge-Kutta method and stopped when the maximum our-of-balance reaction reached a magnitude value less or equal to 0.0001 Newton. At this point, the corresponding vertical displacement (Δ_v) and horizontal longitudinal displacement (Δ_h) of the cantilever's free end, were recorded for each analysis thus reproduced in Table 1. Nothing that, a further element (in addition to those indicated in Table 1) was added at the clamped end of the 3 DoF cantilever model in order to restrain the rotational Degree of Freedom. As it can be seen, the discrepancy between the two formulations (in terms of displacements) is diminishing as the element size reduces. In particular, the 6 DoF formulation is shown to be less sensitive with regard to the element size, nonetheless, for an element size of 208.333 mm the discrepancy in terms of deflection (Δ_h) between the two models is only 63.312 mm on an overall deflection of circa 3 m (i.e. $\approx 2.1\%$).

A torsional displacement $\varphi_L = 90°$ it is also applied in a second analysis step to the 3 DoF cantilever model with 12 elements. The torsion is imposed by increments of 10° at the beam's free end. As shown in Figure 11, the beam undergoes lateral buckling according to the incrementation of the torsional displacement φ_L.

4.2. Application example

The following example aims to illustrate one of the many possible applications, of the described discrete elastic rod model, within the context of actively bent structures. The design problem under consideration consists of finding a 'suitable' geometry for a post-formed grid-shell of the kind illustrated in Figure 1, in order

Element size	Num. of	Δ_v/L^a		Δ_h/L	
[mm]	Elements	3DoF	6DoF	3DoF	6DoF
833.333	12	0.3339	0.3016	0.6697	0.5633
416.666	24	0.3168	0.3017	0.6126	0.5641
277.777	36	0.3112	0.3017	0.5944	0.5642
208.333	48	0.3080	0.3017	0.5928	0.5643

[a] L =10m

Table 1: Vertical and horizontal deflection of cantilever beam for different element sizes and formulations.

to cover a (26 m long by 14 m wide) rectangular area. As shown in Figure 12a, the covering area is firstly subdivided by a mesh made of 32 × 17 quadrilateral elements, thus with each quadrilateral made up by four edges with a uniform length of circa 0.8 m. Following Harding and Shepherd [49] the described mesh is then 'relaxed' by applying a (fictitious) anti-gravitational load at each node and assuming a *zero-length* spring behaviour for each edge of the mesh, with masses proportional to edge-length. The resulting *funicular* discrete geometry, reported in Figure 12b, is then interpolated by a continuous surface and a second analysis step is run, by assuming this time, real axial stiffness values with uniform unstressed length (for the single edge) of 1 m, as well as introducing free body shears reactions, in order to take bending/torsional stiffnesses into account. As in [50] during this second analysis step, a normal-to-surface component of the residual forces $\bar{R}_i$ is computed at each time increment and subtracted from the residual, in order to constrain the mesh relaxing along the funicular surface previously found. The geometry resulting at analysis completion is shown in Figure 12c. The geometry exceeding the rectangular (covering) area is then removed, thus a final geometry is eventually found (Figure 12d).

The explicit fourth-order Runge-Kutta method was adopted for this example, for numerical integration of the acceleration terms.

5. Conclusions

Active-Bending represents an interesting concept, by which, significantly complex geometries can be realised with relatively 'simple' (standardised) connection

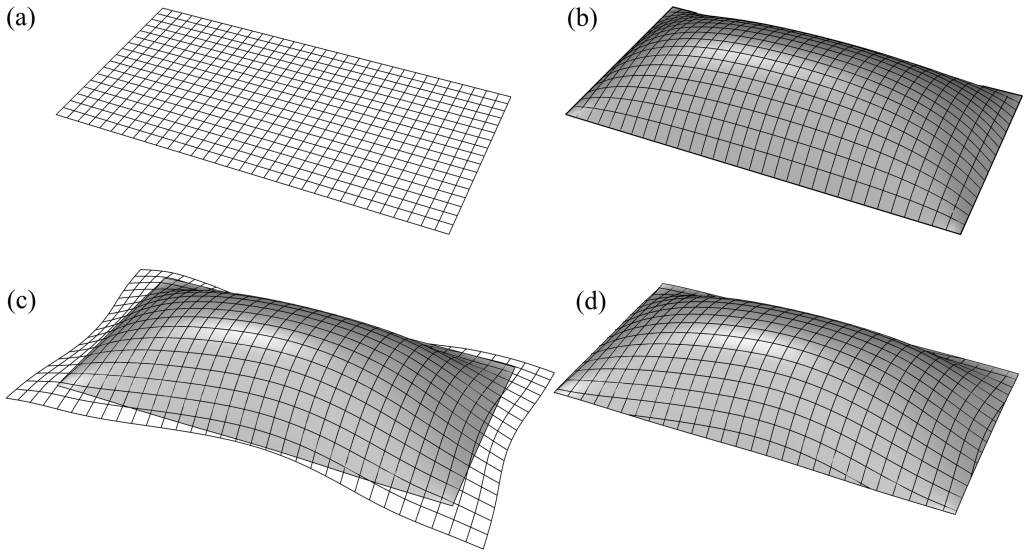

Figure 12: Post-formed grid-shell: (a) Initial flat geometry; (b) Funicular geometry; (c) Funicular geometry with constant edge-length = 1 m; (d) Removing excess geometry.

systems. Nonetheless, the reduction of complexity at a manufacturing level is somehow 'recovered' at a design stage level, meaning that: numerical models become an essential design tool, not only for structural verification/validation purposes, but especially, to assist geometric modelling and shape exploration at initial design stage. According to Pottmann et al [1] the development of numerical models and tools to assist the design process of free-form architectures, can be seen as a discipline on its own, namely: Architectural Geometry.

Within the general framework of such a 'novel' discipline, the main aim of this paper has been to provide an efficient numerical tool for computer simulation of elastic rods, in order to assist and facilitate the form finding and analysis of actively bent structures. The development of discrete elastic rods is a very active and long-standing research topic, constantly leading practical applications in several and disparate sectors. By establishing 'practical' requirements, in terms of: numerical convergence and accuracy, ease of implementation and range of applicability; a 'design-oriented' discrete elastic rod formulation was introduced in here. Such a formulation is entirely described by vector-based quantities, allowing for a (easy) node-by-node implementation, and a reduced number of DoF in order to avoid numerical stiffness associated with rotational DoF. The adoption of a Bishop

(parallel transported) frame to describe the material cross-section orientation and a quasi-static treatment of the twisting DoF, made possible to reduce, in practice, to only three (translations) the number of DoF the be explicitly computed, whilst removing theoretical limitations of 'applicability', typical of translational-only formulations, thus allowing the general case of initially straight rods with torsional stiffness and cross-section anisotropy to be taken into account. From this point of view, the described formulation ambitiously aimed to represents a 'follow-up' contribution to previous, pioneering works [31] on the form finding and analysis of lightweight spline structures. Although not 'as accurate' as DR Finite-Element formulations with 6 DoF (as for instance the one proposed in [40]) the described Finite-Difference formulation represents a valid trade-off in terms of accuracy level and computational time, hence very suitable to be implemented as an interactive numerical tool for design exploration of actively bent structural systems, such as grid-shells.

6. Acknowledgements

The Centre for Timber Engineering (CTE) and the School of Engineering and Built Environment (SEBE), Edinburgh Napier University, are greatly acknowledged for providing the financial support for this research.

References

[1] H. Pottmann, M. Eigensatz, A. Vaxman, J. Wallner, Architectural geometry, Computers & Graphics.doi:http://dx.doi.org/10.1016/j.cag.2014.11.002.

[2] D. Piker, Kangaroo: Form finding with computational physics, Architectural Design (2013) 245–252.doi:http://dx.doi.org/10.1201/b15267-32.

[3] S. Pone, S. Colabella, B. D'Amico, D. Lancia, A. Fiore, B. Parenti, Timber post-formed gridshell: Digital form-finding / drawing and building tool, in: Proc. of the IASS Symposium, Wroclaw, Poland, 2013. doi:http://dx.doi.org/10.13140/2.1.1339.1686.

[4] B. DAmico, A. Kermani, H. Zhang, A form finding tool for post formed timber grid shells, in: proceedings of the World Conference on Timber Engineering, Quebec City, Canada, 2014. doi:http://dx.doi.org/10.13140/2.1.3949.8888.

[5] S. Ahlquist, T. Kampowski, O. O. Torghabehi, A. Menges, T. Speck, Development of a digital framework for the computation of complex material and morphological behavior of biological and technological systems, Computer-Aided Design 60 (2015) 84–104. doi:http://dx.doi.org/doi:10.1016/j.cad.2014.01.013.

[6] S. Nabaei, O. Baverel, Y. Weinand, Form finding of twisted interlaced structures: A hybrid approach, Advances in Architectural Geometry 2014 (2015) 127–143doi:dx.doi.org/10.1007/978-3-319-11418-7_9.

[7] J. Lienhard, H. Alpermann, C. Gengnagel, J. Knippers, Active bending, a review on structures where bending is used as a self-formation process, International Journal of Space Structures 28 (3) (2013) 187–196. doi:http://dx.doi.org/10.1260/0266-3511.28.3-4.187.

[8] P. Oliver, Encyclopedia of vernacular architecture of the world, Cambridge University Press, 1997.

[9] O. Baverel, J.-F. Caron, F. Tayeb, L. D. Peloux, Gridshells in composite materials: Construction of a 300 mq forum for the solidays' festival in paris, Structural Engineering International 22 (3) (2012) 408–414. doi:http://dx.doi.org/10.2749/101686612X13363869853572.

[10] L. du Peloux, F. Tayeb, O. Baverel, J. Caron, Faith can also move composite gridshells, in: Proc. of the IASS Symposium, Wroclaw, Poland, 2013.

[11] E. Happold, W. Liddell, Timber lattice roof for the mannheim bundesgartenschau, The structural engineer 53 (3) (1975) 99–135.

[12] R. Harris, J. Romer, O. Kelly, S. Johnson, Design and construction of the downland gridshell, Building Research & Information 31 (6) (2003) 427–454. doi:http://dx.doi.org/10.1080/0961321032000088007.

[13] R. Harris, S. Haskins, J. Roynon, The savill garden gridshell: design and construction, The Structural Engineer 86 (17) (2008) 27–34.

[14] M. Fleischmann, A. Menges, Icd/itke research pavilion: A case study of multi-disciplinary collaborative computational design, in: Computational Design Modelling, Springer, 2012, pp. 239–248.

[15] P. Nicholas, E. L. Hernández, C. Gengnagel, The faraday pavilion: activating bending in the design and analysis of an elastic gridshell, in: Proceedings of the Symposium on Simulation for Architecture & Urban Design, Society for Computer Simulation International, 2013, p. 21.

[16] D. Naicu, R. Harris, C. Williams, Timber gridshells: Design methods and their application to a temporary pavilion, in: World Conference on Timber Engineering, 2014.

[17] P. Tornabell, E. Soriano, R. Sastre, Pliable structures with rigid couplings for parallel leaf-springs: a pliable timber torus pavilion, Mobile and Rapidly Assembled Structures IV 136 (2014) 117.

[18] J. Harding, W. Pearson, H. Lewis, S. Melville, The ongreening pavilion, in: Advances in Architectural Geometry 2014, Springer, 2015, pp. 295–308.

[19] M. Fleischmann, J. Knippers, J. Lienhard, A. Menges, S. Schleicher, Material behaviour: embedding physical properties in computational design processes, Architectural Design 82 (2) (2012) 44–51. doi:http://dx.doi.org/10.1002/ad.1378.

[20] A. Patriciu, D. Mazilu, H. S. Bagga, D. Petrisor, L. Kavoussi, D. Stoianovici, An evaluation method for the mechanical performance of guide-wires and catheters in accessing the upper urinary tract, Medical Engineering & Physics 29 (8) (2007) 918–922. doi:http://dx.doi.org/10.1016/j.medengphy.2006.09.002.

[21] T. Schlick, Modeling superhelical dna: recent analytical and dynamic approaches, Current opinion in structural biology 5 (2) (1995) 245–262. doi:http://dx.doi.org/10.1016/0959-440X(95)80083-2.

[22] J. Spillmann, M. Teschner, C o r d e: Cosserat rod elements for the dynamic simulation of one-dimensional elastic objects, in: Proceedings of the 2007 ACM SIGGRAPH/Eurographics symposium on Computer animation, Eurographics Association, 2007, pp. 63–72.

[23] M. Bergou, M. Wardetzky, S. Robinson, B. Audoly, E. Grinspun, Discrete elastic rods, in: ACM Transactions on Graphics (TOG), Vol. 27, ACM, 2008, p. 63. doi:http://dx.doi.org/10.1145/1399504.1360662.

[24] N. Umetani, R. Schmidt, J. Stam, Position-based elastic rods, in: ACM SIGGRAPH 2014 Talks, ACM, 2014, p. 47. doi:http://dx.doi.org/10.1145/2614106.2614158.

[25] S. Siu, L. Rhode-Barbarigos, S. Wagner, S. Adriaenssens, Dynamic relaxation study and experimental verification of dielectric-elastomer minimum-energy structures, Applied Physics Letters 103 (17) (2013) 171906.

[26] A. Theetten, L. Grisoni, C. Andriot, B. Barsky, Geometrically exact dynamic splines, Computer-Aided Design 40 (1) (2008) 35–48. doi:http://dx.doi.org/10.1016/j.cad.2007.05.008.

[27] M. Grégoire, E. Schömer, Interactive simulation of one-dimensional flexible parts, Computer-Aided Design 39 (8) (2007) 694–707. doi:http://dx.doi.org/10.1016/j.cad.2007.05.005.

[28] K.-J. Bathe, S. Bolourchi, Large displacement analysis of three-dimensional beam structures, International Journal for Numerical Methods in Engineering 14 (7) (1979) 961–986. doi:http://dx.doi.org/10.1002/nme.1620140703.

[29] J. C. Simo, L. Vu-Quoc, On the dynamics in space of rods undergoing large motions: a geometrically exact approach, Computer methods in applied mechanics and engineering 66 (2) (1988) 125–161. doi:http://dx.doi.org/10.1016/0045-7825(88)90073-4.

[30] S. M. L. Adriaenssens, Stressed spline structures., Ph.D. thesis, University of Bath (2000).

[31] S. Adriaenssens, M. Barnes, Tensegrity spline beam and grid shell structures, Engineering structures 23 (1) (2001) 29–36. doi:http://dx.doi.org/10.1016/S0141-0296(00)00019-5.

[32] M. R. Barnes, S. Adriaenssens, M. Krupka, A novel torsion/bending element for dynamic relaxation modeling, Computers & Structures 119 (2013) 60–67. doi:http://dx.doi.org/10.1016/j.compstruc.2012.12.027.

[33] D. Baraff, A. Witkin, Large steps in cloth simulation, in: Proceedings of the 25th annual conference on Computer graphics and interactive techniques, ACM, 1998, pp. 43–54. doi:http://dx.doi.org/10.1145/280814.280821.

[34] M. R. Barnes, Form finding and analysis of tension structures by dynamic relaxation, International journal of space structures 14 (2) (1999) 89–104. doi:http://dx.doi.org/10.1260/0266351991494722.

[35] S. Pone, B. D'Amico, S. Colabella, B. Parenti, D. Lancia, A. Fiore et al, Construction and form-finding of a post-formed timber grid-shell, in: Structures and architecture. Concepts, Applications and challenges, 2013, pp. 245–252. doi:http://dx.doi.org/10.1201/b15267-32.

[36] G. Kirchhoff, Ueber das gleichgewicht und die bewegung eines unendlich dünnen elastischen stabes., Journal für die reine und angewandte Mathematik 56 (1859) 285–313.

[37] E. Cosserat, F. Cosserat, Théorie des corps déformables, Paris (1909).

[38] S. S. Antman, The theory of rods, in: Linear Theories of Elasticity and Thermoelasticity, Springer, 1973, pp. 641–703. doi:http://dx.doi.org/10.1007/978-3-662-39776-3_6.

[39] F. Frenet, Sur les courbes à double courbure., Journal de Mathématiques pures et appliquées (1852) 437–447.

[40] B. D'Amico, A. Kermani, H. Zhang, Form finding and structural analysis of actively bent timber grid shells, Engineering Structures. 81 (2014) 195–207. doi:http://dx.doi.org/10.1016/j.engstruct.2014.09.043.

[41] K.-J. Bathe, Finite element procedures, Klaus-Jurgen Bathe, 2006.

[42] P. Cundall, Explicit finite-difference method in geomechanics, Numerical Methods in Geomechanics, ASCE, (1976).

[43] M. R. Barnes, Non-linear numerical solution methods for static and dynamic analysis of tension structures, Air-supported Structures: the State of the Art, Institution of Structural Engineers, London (1980) 8–56.

[44] R. Bartels, J. Beatty, B. Barsky, Hermite and cubic spline interpolation, An Introduction to Splines for Use in Computer Graphics and Geometric Modelling (1998) 9–17.

[45] E. Catmull, R. Rom, A class of local interpolating splines, Computer aided geometric design 74 (1974) 317–326.

[46] R. L. Bishop, There is more than one way to frame a curve, American Mathematical Monthly (1975) 246–251.

[47] A. J. Hanson, H. Ma, Parallel transport approach to curve framing, Indiana University, Techreports-TR425 11 (1995) 3–7.

[48] B. DAmico, A. Kermani, H. Zhang, P. Shepherd, C. Williams, Optimization of cross-section of actively bent grid shells with strength and geometric compatibility constraints, Computers & Structures 154 (2015) 163–176. doi:http://dx.doi.org/10.1016/j.compstruc.2015.04.006.

[49] J. Harding, P. Shepherd, Structural form finding using zero-length springs with dynamic mass, in: 2011 IASS Annual Symposium: IABSE-IASS 2011: Taller, Longer, Lighter, University of Bath, 2011.

[50] C. J. K. Williams, The analytic and numerical definition of the geometry of the british museum great court roof, in: Mathematics & design 2001, Deakin University, 2001, pp. 434–440.